Available online at www.sciencedirect.com
ScienceDirect
Biomedical Signal Processing and Control 3 (2008) 67–77
Biomedical Signal Processing and Control
www.elsevier.com/locate/bspc

T-wave width as an index for quantification of ventricular repolarization dispersion: Evaluation in an isolated rabbit heart model

Pedro D. Arini [a,*], Guillermo C. Bertrán [b], Esteban R. Valverde [c], Pablo Laguna [d]

[a] *Instituto Argentino de Matemática, CONICET, Buenos Aires, Argentina*
[b] *Instituto de Investigaciones Médicas Dr. A. Lanari, Universidad de Buenos Aires, Buenos Aires, Argentina*
[c] *Facultad de Ingeniería, Universidad de Buenos Aires, Buenos Aires, Argentina*
[d] *Instituto de Investigaciones en Ingeniería de Aragón, CIBER-BNN, Universidad de Zaragoza, Zaragoza, Spain*

Received 26 February 2007; received in revised form 20 September 2007; accepted 4 October 2007

Abstract

This study examined the significance of ECG-derived indexes in quantifying ventricular repolarization dispersion (VRD) given its value as a risk marker for severe myocardial arrhythmia. Multilead ECG recordings from an isolated rabbit heart model, including control and globally increased VRD (IVRD) beats, were studied. The IVRD was induced by supplying d-Sotalol (DS) or premature ventricular stimulation (PVS). ECG indexes came from (a) the absolute ECG summation signal, from which we obtained the amplitude and area of the T-wave, and the T-wave width (T_W), which we consider as IVRD indexes, and (b) the Singular Value Decomposition (SVD) of the ECG, from which the θ_{PT} (angle between the first SVD principal axis and the repolarization axis), T-wave residuum (T_{WR}), T-wave morphology dispersion (T_{MD}), unnormalized T_{MD} (UT_{MD}), and θ_{RT} (the angle between the depolarization and the repolarization vectors) were estimated as IVRD indexes. Results were compared with the classical QT-based VRD indexes (σ_{QT_e}, standard deviation of QT end). The main results are T_W: 78.0 ± 10.3 vs. 133.6 ± 29.6 ms, for control vs. IVRD generated using DS, $p < 0.005$ and 95.2 ± 7.9 vs. 118.5 ± 15.7 ms when PVS was used, $p < 0.007$; σ_{QT_e}: gives 6.5 ± 1.4 vs. 11.6 ± 1.9 ms, for DS $p < 0.007$ and 7.6 ± 2.2 vs. 13.0 ± 3.4 ms for PVS, $p < 0.007$; respectively. θ_{PT}: $35 \pm 51°$ vs. $117 \pm 49°$, $p < 0.009$ in DS. We concluded that globally induced IVRD is well reflected by the T_W parameter, being the most sensitive of the studied ones. The IVRD can also be quantified by using the θ_{PT} index.

Keywords: Electrocardiography; T-wave; SVD; Repolarization heterogeneity; Arrhythmia

1. Introduction

Experimental and clinical studies have demonstrated a relationship between ventricular repolarization dispersion (VRD) and severe ventricular arrhythmia and/or sudden death [1,2]. In addition, patients having VRD values that are higher than normal have a higher risk of developing reentrant arrhythmias [3–6]. Both the QT interval dispersion (QT_d), measured as the difference between the maximum and minimum QT interval values among all of the leads (Δ_{QT}) [7], and the QT standard deviation (σ_{QT}) of the standard 12-lead electrocardiogram (ECG) [8,9] have been proposed as indexes for quantifying VRD. QT_d was proposed as a regional marker of VRD, if it is assumed that each ECG lead mainly records the local activity at different myocardium areas [10]. In a study that used an isolated heart rabbit preparation [11], the QT and JT interval dispersions were significantly correlated with the action potential duration (APD) dispersion. Moreover, that phenomenon was confirmed in human subjects given the high correlation between the 24-h QT_d and the intracardiac monophasic APD dispersion [12]. Clinical studies have shown that the QT_d is a predictor of arrhythmia in congenital long-QT syndrome patients [13] and is used to evaluate the risks of proarrhythmia effect class III antiarrhythmic drugs [14]; however, the nature of the relationship between QT_d and VRD is controversial because of technical issues [15,16] (involving the computation of the QT interval) and conceptual problems associated with QT_d [17]. Several studies suggest that the result of the measurement can be affected by inaccuracies in the determination of the T-wave end, the existence of U-wave

* Corresponding author. Tel.: +54 11 49546781.
E-mail address: pedroarini@yahoo.com.ar (P.D. Arini).

1746-8094/$ – see front matter © 2007 Elsevier Ltd. All rights reserved.
doi:10.1016/j.bspc.2007.10.001

and notched T-waves [8,18]. On the other hand, the main problems with determining increased VRD (IVRD) using QT_d are the effects generated by the projections of T-wave loops that have different shapes and different angles onto the axis of each ECG lead, which results in T-waves that have different amplitudes and morphologies [17]. Besides, the QT_d measured using a standard 12-lead ECG was compared to the QT_d measured using the synthesized 12 leads from the orthogonal XYZ leads [19,20], which did not show the effects of regional heterogeneity. The results of the two approaches did not differ significantly, questioning the hypothesis which supports the clinical value of QT_d. Other studies have shown that QT_d differed significantly between patients that had a wide T-wave loop and those that had a narrow T-wave loop and, in consequence a correspondence between the QT_d and the T-wave loop morphology was observed [17].

Another way to analyze ECG signals for the evaluation of the VRD is to work into a minimum dimensional space determined using ECG Singular Value Decomposition (SVD) [21–23]. The transformed ECG data can be used to estimate descriptors and indexes for the detection and quantification of the pathological characteristics of ventricular repolarization [24–26]. The total cosine R-to-T (T_{CRT}) descriptor calculates the cosine angle between the depolarization and repolarization dominant vectors in a three-dimensional (3D) loop [23]. In this study we will consider the angle θ_{RT} rather than the cosine. The T-wave morphology dispersion (T_{MD}) descriptor [23] calculates the mean angular dispersion between all pairs of leads at the T-wave interval. In addition, the T-wave residuum (T_{WR}) index evaluates the relationship between the first three SVD components (as the dipolar cardiac electrical vector representation) and the non-dipolar components (which are assumed to be related to the local heterogeneity of the myocardium) [25]. Other authors [27] used isolated-perfuse canine hearts to measure QT_d and T-wave width from the root-mean-square (RMS) curve obtained from: the available epicardial electrograms, ECG body surface leads, standard precordial ECG leads, and optimal lead set. They induced myocardial repolarization dispersion by changing temperature, cycle length, and activation sequence. The VRD, which was measured directly using recovery times from epicardial potentials, was compared to T-wave width and QT_d. VRD was strongly correlated with T-wave width computed from the RMS series, but not with the classical QT_d. In our study, we tested the hypothesis that T-wave width (T_W) measured at the surface ECG is a better marker of IVRD than other markers derived from temporal and geometric analyses. In the early analysis of VRD the apico-basal voltage gradient was the assumed responsible of the T-wave morphology [28]. Recent investigations have demonstrated that the apico-basal voltage gradient collaborate little to the T-wave manifestation on the ECG [29]. However, it is necessary to stress that in [30], the authors expressed in 'Limitations of the Study' that the data presented do not allow a total evaluation of the extent to which apico-basal or antero-posterior versus transmural gradients contribute to the ECG. Then, it is necessary to assume that T-wave widening can result from both, a transmural or global dispersion. We founded our hypothesis in the fact that IVRD should be reflected at the surface ECG as a increase in T-wave width. We showed in Fig. 1, one likely T-wave generation as a result of combined dispersion between apex-base and

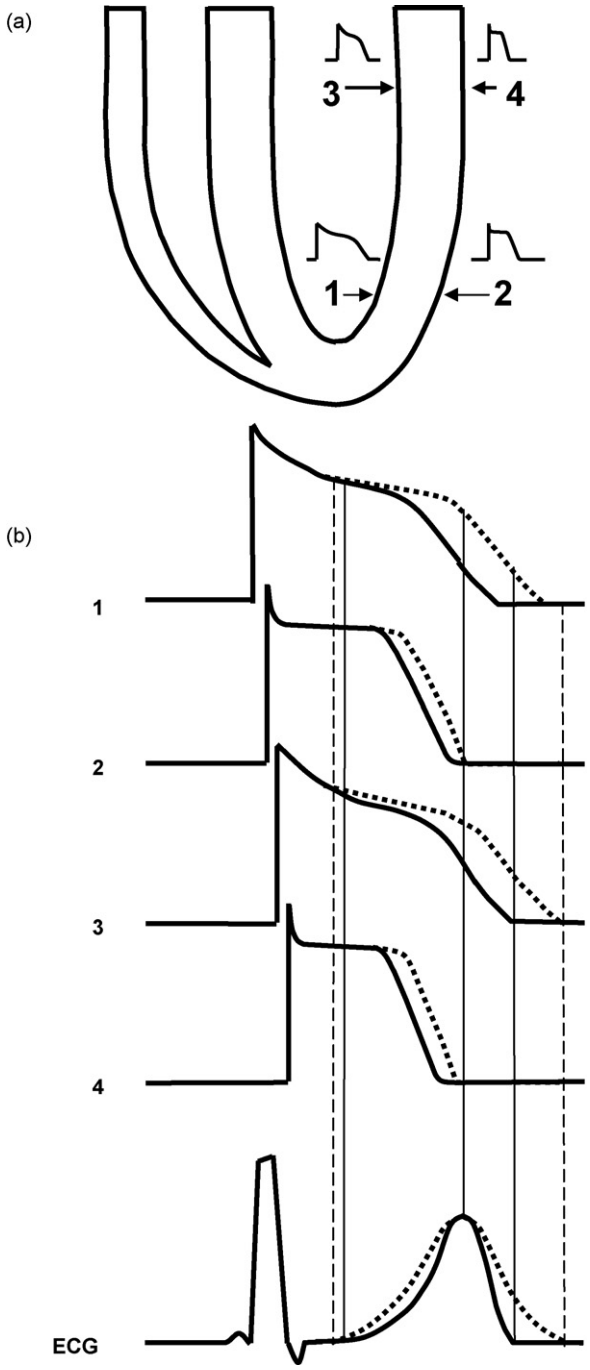

Fig. 1. Example of an increase in T-wave width in a surface ECG. Schematic picture representing the T-wave generation as a result of combined dispersion between apex to base and transmural. Increased dispersion at any of these types can result in T-wave widening. However, there is not proof about T-wave width in rabbits comes from transmural or apico-basal dispersion. This pictures should be seen just as a scheme to understand the hypothesis of the T-wave widening no matter if it comes from one or other dispersion type. (a) Schematic diagram of the ventricles with its endocardial and epicardial action potential (AP) in the base and apex. (b) Schematic drawing of the AP and ECG with control (solid line) and during VRD increases (dotted line).

transmural APD. Increased dispersion at any or both of these types can result in T-wave widening. Since, in our investigation, the gold standard is its own control any increase in T-wave width should be consequence of dispersion either transmural or global.

To that end, we used the addition of d-Sotalol (DS) [30,6,31,32] and premature ventricular stimulation (PVS) [33–37] to induce IVRD artificially in an isolated in vitro rabbit heart model. The ECG-derived indexes based on temporal analyses were obtained from a signal resulting from the summation of the absolute values of all the ECG leads in a multi-electrode recording system. In addition, the classical measurements of the QT_d were calculated. Geometrical indexes were calculated as the T_{WR}, T_{CRT}, T_{MD}, UT_{MD} (unnormalized T-wave morphology dispersion) and θ_{PT} (the total cosine main axis to T-wave angle) obtained from SVD of the lead set systems. We tested the hypothesis that T_{WR} does not reflect increases in VRD generated globally (across the whole myocardium) and that the T_W better reflects the increase in VRD, when compared to T_{CRT}, T_{WR}, UT_{MD} and T_{MD}.

2. Materials and methods

2.1. Isolated heart rabbit preparation

This study conformed to the *Guide for the Care and Use of Laboratory Animals* published by the US National Institutes of Health (NIH Publication No. 85-23, revised 1996). To obtain isolated Langendorff-perfused rabbit hearts, male New Zealand white rabbits of 2.8–3.8 kg ($n = 20$) were heparinized (500 U/kg IV) and anesthetized by the intramuscular injection of a combination of lidocaine (5 mg/kg) and ketamine (35 mg/kg). The rabbits were euthanized by cervical dislocation. The chest was opened via a median sternotomy and, immediately, the heart was removed with scissors and immersed in cold Tyrode's solution. After the remaining connective tissue, lungs, and pericardium were removed, the heart was placed in a vertical Langendorff device through cannulation of the aorta. Time from chest opening to cannulation of the aorta oscillated between 2 and 3 min. The heart was retrogradely perfused through the aorta with Tyrode's solution and immersed in a tank filled with the same solution [11]. The temperature of both solutions were maintained at 38 ± 0.5°C and bubbled with O_2 using a flow of 700–900 ml/h at a pressure of 70 mmHg. To regulate the flow rate of the aortic perfusion, a variable speed roller pump (Extracorporeal, 2102 Infusion Pump) was used. Care was taken to fix the hearts in the same position by alignment of the left anterior descending coronary artery (LAD) with the electrode matrix reference system on the tank.

The composition of Tyrode's solution was (in mM): 140 NaCl, 5 KCl, 1 $MgCl_2$, 0.33 NaH_2PO_4, 5 Hepes, 11.1 glucose and 2 $CaCl_2$. The pH was adjusted to 7.4 using NaOH. The sinus node was destroyed by applying radiofrequency energy through a customized device. In both of the experimental protocols, DS supply and PVS, the artificial pacemaker was a rectangular pulse that had a 2 ms duration and twice the

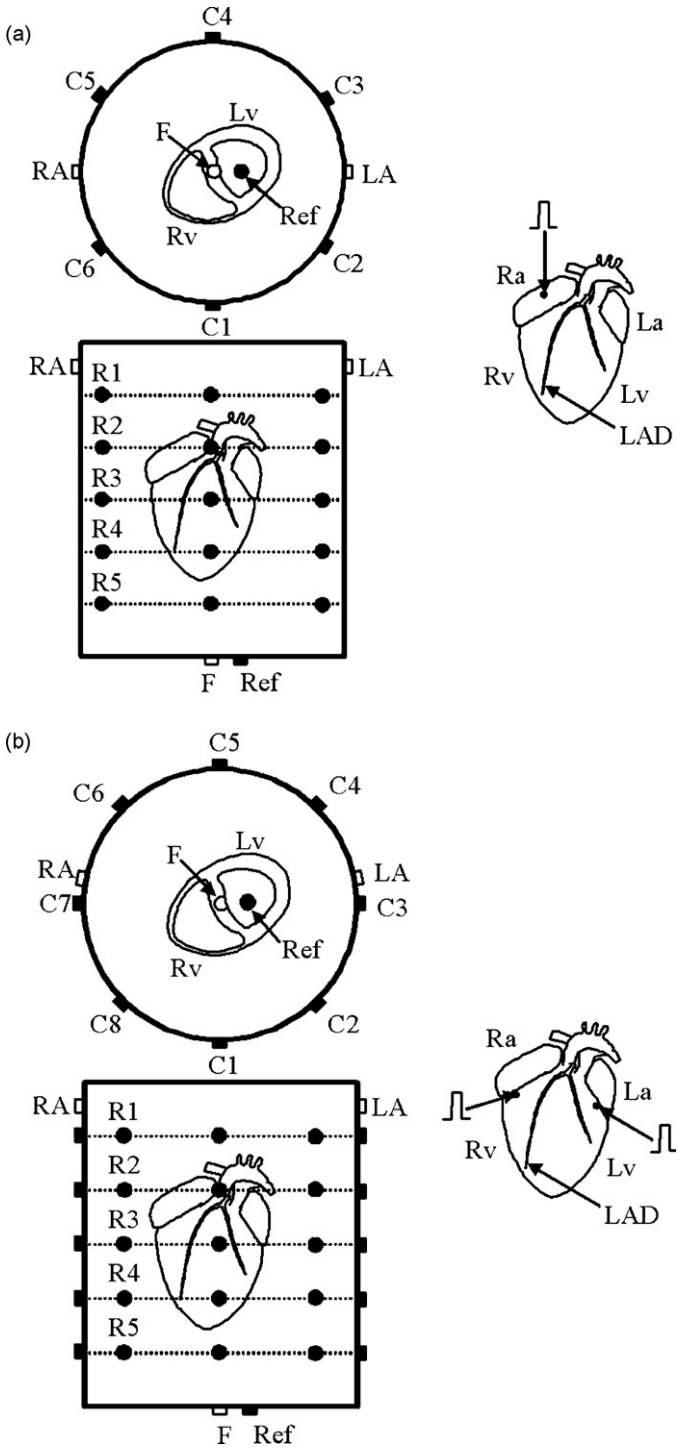

Fig. 2. (a) 30-electrode configuration for electrocardiographic recording in the d-Sotalol protocol. Schematic view showing the superior and frontal 5 × 6 matrix electrodes, as well as the standard lead foot (F), left arm (LA), right arm (RA), and reference (Ref). Also is shown the stimulation site from the right auricle (Ra), the left auricle (La), the left ventricle (Lv), the right ventricle (Rv), and the left anterior descending coronary artery (LAD). (b) 40-electrode configuration for electrocardiographic recording in the premature ventricular stimulation protocol. Also are shown the positions of both of the stimulating electrodes located in the base of the Lv and Rv, below the atrial appendages.

diastolic threshold stimuli amplitude. In the DS experimental protocol, the bipolar pacing electrodes made of Teflon-coated stainless-steel wires were positioned in the right auricle (Fig. 2 a) and, in the PVS experimental protocol, in the middle of the base of each ventricle, below the auricle appendage (Fig. 2b). To ensure stability in the preparation, the heart activity was monitored for 30 min to determine that the heart was arrhythmia-free, stable in amplitude, and had no manifest ischemia. We used an in vitro rabbit heart model because it provides advantages such as a high level of experimental reproducibility, has a greater throughput compared to complicated in vivo models, provides a better evaluation over a range of concentrations and different combinations of drugs to be tested. In addition, it can be manipulated to mimic clinical conditions, such as hypokalemia and bradycardia that support this comments. No attempt was made to measure heterogeneities of ventricular repolarization on the epicardial surface or endocardial muscle layers. We limited our analysis to ECG signals obtained from recording electrodes embedded in the tank wall. It has been well established that with PVS beats [38] or by supply DS doses $> 10\mu M$ [31] a significant increase in ventricular repolarization dispersion is induced.

2.2. Thorax rabbit model

The experimental model consisted of the in vitro system, which used a multiple recording system to obtain the beat-to-beat electrical activity of isolated rabbit heart. We used two experimental protocols. The DS protocol used a circular tank (diameter = 10 cm, height = 10 cm) that had 30 silver–silver chloride electrodes (diameter = 2 mm) distributed homogeneously. All of the electrodes were mounted on the wall of the tank in an array of five rows (interelectrode distance = 15 mm) and six columns (angular distance between electrodes 60°) (Fig. 2a). The PVS protocol used a circular tank (diameter = 7 cm, height = 7cm) that had 40 silver–silver chloride electrodes distributed homogeneously within an array of 5 rows and 8 columns (see Fig. 2b). The distance between electrodes was 10 mm and the angular distance was 45°. The dimensions of the tank simulated a rabbit's thorax. In both protocols, four additional electrodes were allocated in an *"Einthoven-like"* configuration (Fig. 2). Two of them were positioned on the base of the tank and the other two were on the upper left and right side of the tank wall and served as arm electrodes. The four electrodes were designed to build the electrical reference by configuring the Wilson Central Terminal.

2.3. Experimental protocols

In this study VRD was increased by supplying DS [31,39] or by PVS [40,38]. Due to heterogeneous distribution of APD lengthening induced by potassium-channel blocking drugs [31,41] or the heterogeneous shortening of APD caused by the heterogeneous distribution of restitution kinetics [38], a real IVRD phenomena can be obtained. Besides, it can be noted that we measured the increase in VRD, not dispersion as an absolute value, so our gold standard was the same heart in the control condition in each experiment.

In the DS protocol, Tyrode's solution was perfused for a control period (C_{DS}) of 30 min; then, to generate increased dispersion, DS solution (60 μM) was perfused during the increased dispersion period (D_{DS}). The ECG was recorded during C_{DS} and D_{DS} and the derived variables measured.

In the PVS protocol, the heart was stimulated from the right ventricle (Rv) or left ventricle (Lv) at basal frequency during a train (S1) of 49 beats. After that train, at beat number 50th, a premature beat was generated at a coupling interval that corresponded to the Effective Refractory Period (E_{rp}) plus 5 ms. In each case, E_{rp} was estimated prior to the PVS application. To estimate E_{rp}, premature coupling intervals (distance from the last beat to the premature stimulation time) were diminished step by step at 5 ms until period refractoriness was reached. We used the average of 48th and 49th beats from each S1 as control (C_{PVS}). The premature beat (50th) was elicited to generate dispersion paced either at Rv or Lv (D_{PVS}).

In both of the protocols, the heart was paced using an artificial pacemaker (DTU 101, Bloom Associates Ltd., Reading, PA, USA). In the DS protocol ($n = 10$), the hearts were paced from the right auricle at a basic cycle length of 500 ms to prevent electrical unstationary activity generated by a spontaneous heart rate. In the PVS protocol ($n = 10$), the hearts were paced from the Rv ($n = 5$) or the Lv ($n = 5$) by stimuli trains at a basic cycle length of 400 ms for control condition. Then, single premature stimuli were applied after a pulse train at a frequency equal to $E_{rp} + 5$ ms (167 ± 7.2 ms for Rv stimulation and 168 ± 11.5 ms for Lv stimulation; p = NS).

To quantify to which extent the stability is guaranty we did measure the coefficient of variation (C_V) parameter [42] for each feature, the QT_{end}, QT_{peak}, QRS duration, T-wave amplitude, T-wave area (measures as in [37]) and T-wave onset, T-wave peak position, T-wave end (measures as in [43]). These variables were repeatedly measured at each electrode of the multi-lead ECG recording system every 20 min during an hour. The C_V is defined as

$$C_V = \sqrt{\sigma^2} \times 100\% \tag{1}$$

and the σ^2 (variance within) is estimated as

$$\sigma^2 = \sum_{i=1}^{k} \sum_{j=1}^{n_i} \frac{(y_{ij} - \bar{y}_i)^2}{n - k} \tag{2}$$

For each variable evaluated (QT_{end}, QT_{peak}, QRS, T-wave amplitude,T-wave area, T-wave onset, T-wave peak position and T-wave end) we assume that there are k groups of measurements with n_i measurements in the ith group. The jth measurements in the ith group will be denoted by y_{ij} and $n = \sum_{i=1}^{k} n_i$. The term $(y_{ij} - \bar{y}_i)$ represents the deviation of an individual measurement from the group mean for that measurement and is a clue of within group variability. In some experiments, we evaluated the C_V for each variable. The C_V was <2% for QT_{end}, <1.5% for QT_{peak}, <2% for QRS, <5% for T-wave amplitude, <5% for T-wave area, <5% for T-wave onset, <2% for T-wave peak position and <2% T-wave

end. So, we verified that the estimated variables did not shown significant statistical differences over the 1-h in vitro experiment.

2.4. Acquisition

ECG data were recorded using instrumentation amplifiers that had a gain factor of 1000 and a bandwidth of 0.05–300 Hz. The signals were digitalized at a sampling rate $f_s = 1000$ Hz and 12-bit resolution using a digital acquisition board (Lab PC+, National Instruments, Austin, TX, USA). When necessary, a band-stop filter was used to remove 50-Hz. The baseline movement was compensated using a cubic spline [44] algorithm. All of the data were acquired and monitored using customized software made in C++.

2.5. Methods of analysis

The ECGs from the first row of leads were recorded simultaneously, and the same procedure was applied sequentially to the remaining rows. The ith beat was selected in the ECG recordings of each rth row, $r = 1, \ldots, 5$, obtaining the i_rth beat. After selecting and segmenting the i_rth beat from each row, a signal, $x_{c,r}(n), n = 0, \ldots, N-1$, was determined for each channel characterized by the (c, r) pair, where c is the column in the electrode matrix $(c = 1, \ldots, L)$ and r is the row. $L = 6$ for the DS protocol and $L = 8$ for the PVS protocol, being $M = 5 \times L$ the number of register electrodes in each experimental protocol, respectively. Expressing that signal as a vector, $\mathbf{x}_{c,r}$, we obtain

$$\mathbf{x}_{c,r} = [x_{c,r}(0), \ldots, x_{c,r}(N-1)]^{\mathrm{T}} \tag{3}$$

The five i_rth selected beats were aligned using the QRS complex maximum upstroke slope. The beats extend a time window compose of N samples corresponding to 400 ms, and include the repolarization phase. For each experimental condition (C_{DS}, D_{DS}, C_{PVS}, D_{PVS}), recordings were obtained from 30 and 40 ECG leads for the DS and PVS protocols, respectively. Expressing in matrix notation the selected segmented signals, $\mathbf{X}(M \times N)$, we obtain

$$\mathbf{X} = [\mathbf{x}_{1,1}, \ldots, \mathbf{x}_{L,1}, \ldots, \mathbf{x}_{1,5}, \ldots, \mathbf{x}_{L,5}]^{\mathrm{T}} \tag{4}$$

From $\mathbf{X}$, the ECG-derived parameters were measured. A matrix $\mathbf{X}$ characterize each experimental condition.

2.5.1. Temporal analysis

The signal from the summation of the *absolute* ECG signal was calculated as

$$x_{\mathrm{A}}(n) = \sum_{c=1}^{L} \sum_{r=1}^{5} |x_{c,r}(n)| \tag{5}$$

We computed the T-wave onset ($n = n_{\mathrm{o}}^{\mathrm{A}}$), T-wave end ($n = n_{\mathrm{e}}^{\mathrm{A}}$) and T-wave peak position ($n = n_{\mathrm{p}}^{\mathrm{A}}$). The upper index A explicitly labels the signal from which the measurement comes and distinguishes among the same measurements coming from other derived signals (see in Fig. 3). The derived indexes are

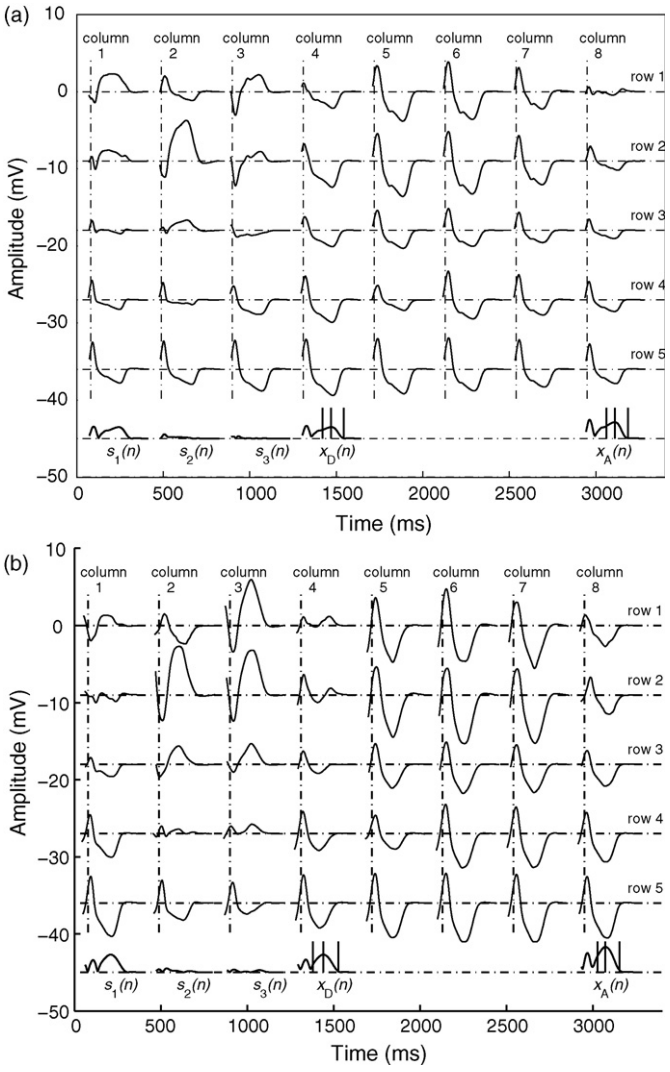

Fig. 3. 40 ECG recordings from the control (C_{PVS}, top panel) and their respective IVRD (D_{PVS}, bottom panel) during PVS from the left ventricle. The stimulating electrode was located at the base of the left ventricle. The last row of both panels shows the first three components, $s_1(n)$, $s_2(n)$, and $s_3(n)$, when SVD is applied. Also, we can see the reconstructed summation of the absolute ECG signals $x_{\mathrm{A}}(n)$ and the module of the cardiac electrical vector under the dipolar SVD $x_{\mathrm{D}}(n)$ with the fiducial points, T-wave onset, T-wave peak and T-wave end; respectively.

- T-wave onset location ($T_{\mathrm{o}}^{\mathrm{A}}$), $T_{\mathrm{o}}^{\mathrm{A}} = n_{\mathrm{o}}^{\mathrm{A}} / f_s$.
- T-wave peak location ($T_{\mathrm{p}}^{\mathrm{A}}$), $T_{\mathrm{p}}^{\mathrm{A}} = n_{\mathrm{p}}^{\mathrm{A}} / f_s$.
- T-wave end location ($T_{\mathrm{e}}^{\mathrm{A}}$), $T_{\mathrm{e}}^{\mathrm{A}} = n_{\mathrm{e}}^{\mathrm{A}} / f_s$.
- T-wave peak maximum amplitude (T_{M}), $T_{\mathrm{M}} = x_{\mathrm{A}}(n_{\mathrm{p}}^{\mathrm{A}})$.
- T-wave width (T_{W}), $T_{\mathrm{W}} = (n_{\mathrm{e}}^{\mathrm{A}} - n_{\mathrm{o}}^{\mathrm{A}}) / f_s$.
- T-wave area (T_{A}), $T_{\mathrm{A}} = \sum_{n=n_{\mathrm{o}}^{\mathrm{A}}}^{n_{\mathrm{e}}^{\mathrm{A}}} x_{\mathrm{A}}(n)$.

$n_{\mathrm{o}}^{\mathrm{A}}$, $n_{\mathrm{e}}^{\mathrm{A}}$, and $n_{\mathrm{p}}^{\mathrm{A}}$, are relative to the QRS reference point and are expressed in sampling values. The fiducial points were detected using a threshold-based algorithm on the differentiated signal [43]. Once the maximum and minimum of the differentiated signal were detected, a threshold K was established to detect the $n_{\mathrm{o}}^{\mathrm{A}}$ at the time location where the differentiated signal fell down by a factor $K = 0.2$ previous to

the maximum slope instant, and by a different factor, $K = 0.8$, posterior to the minimum slope instant to detect the n_e^A. The n_p^A position was determined using the zero-crossing on the differentiated signals. The differentiator filter transfer function was $H(z) = f_s/2(1 - z^{-2})$.

2.5.2. Geometrical analysis

The ECG matrix $\mathbf{X}$ was subjected to SVD [21], therefore: if $\mathbf{X}$ is an $M \times N$ ($M < N$) matrix, with M unipolar electrodes and N samples in the beat, then there are two orthogonal matrices represented as

$$\mathbf{U} = [\mathbf{u}_1, \ldots, \mathbf{u}_M] \in \mathbb{R}^{M \times M} \quad \text{and} \quad \mathbf{V} = [\mathbf{v}_1, \ldots, \mathbf{v}_N] \in \mathbb{R}^{N \times N}$$

such that

$$\Sigma = \mathbf{U}^T \mathbf{X} \mathbf{V} = [\text{diag}(\sigma_1, \ldots, \sigma_M)\, \mathbf{0}] \tag{6}$$

where $\Sigma \in \mathbb{R}^{M \times N}$, $\mathbf{0} \in \mathbb{R}^{M \times (N-M)}$. The singular values, σ_j ($j = 1, \ldots, M$), are ordered such that $\sigma_1 \geq \sigma_2 \geq \sigma_3 \geq \cdots \geq \sigma_M \geq 0$. The columns of $\mathbf{U}$ are refereed to as the left singular vectors and the columns of $\mathbf{V}$ are refereed to as the right singular vectors. Furthermore, if $\sigma_1 \geq \cdots \geq \sigma_p > \sigma_{p+1} = \cdots = \sigma_M = 0$ then, rank $(\mathbf{X}) = p$ and range $(\mathbf{X})$=span $\{\mathbf{u}_1, \ldots, \mathbf{u}_p\}$.

(a) *Depolarization-repolarization angle, θ_{RT}, and repolarization-principal component angle, θ_{PT}*: The parameters that reflect a 3D comparison between repolarization and depolarization wavefronts, were obtained from the minimum decomposition subspace and its corresponding left singular vectors. Then

$$\mathbf{X} = \mathbf{U}\Sigma\mathbf{V}^T = [\mathbf{U}_1\mathbf{U}_2] \begin{bmatrix} \Sigma_1 & \mathbf{0} \\ \mathbf{0} & \Sigma_2 \end{bmatrix} \begin{bmatrix} \mathbf{V}_1^T \\ \mathbf{V}_2^T \end{bmatrix}$$

There are studies showing that 98% of the ECG energy was represented in a 3D subspace [45], in this case, $\mathbf{U}_1 \in R^{M \times 3}$, and $\Sigma_1 \in \mathbb{R}^{3 \times 3}$. Then we used a 3D subspace that was spanned on the three columns of $\mathbf{U}_1$, which was calculated as $\mathbf{S} = \mathbf{U}_1^T \mathbf{X}$. Each column of $\mathbf{S}(3 \times N)$ associated to time instant n is

$$\mathbf{s}(n) = [s_1(n), s_2(n), s_3(n)]^T \tag{8}$$

which is the projection of the M dimensional columns of $\mathbf{X}$. Hence, it is possible to characterize the dependence of ECG into the three main components spanded by $[\mathbf{u}_1, \mathbf{u}_2, \mathbf{u}_3]$, meaning $\mathbf{S} \in \text{span}[\mathbf{u}_1, \mathbf{u}_2, \mathbf{u}_3]$. The rows $s_i(n)$ $i = 1, 2, 3$, are the transformed ECG signals in the three main orthogonal directions (pseudo-leads). In the Fig. 4, the most of the energy was projected on the first five components when SVD was applied, although 98% of the total energy is in the first three components [46].

The algorithm for detecting fiducial points was also applied to the composed signal $x_D(n)$. Let

$$x_D(n) = \sqrt{\sum_{i=1}^{3} s_i^2(n)} \tag{9}$$

The fiducial points T-wave onset ($n_{T,o}^D$), T-wave end ($n_{T,e}^D$), and T-wave peak position ($n_{T,p}^D$) were obtained from $x_D(n)$ (see in Fig. 3). Then, the T-wave matrix was segmented as

$$\mathbf{S}_T = [\mathbf{s}(n_{T,o}^D), \ldots, \mathbf{s}(n_{T,p}^D), \ldots, \mathbf{s}(n_{T,e}^D)] \tag{10}$$

The maximum value of $x_D(n)$ in the first 100 ms is associated with the R-wave peak, $n_{R,p}^D$. From that location, a depolarization QRS wave matrix, $\mathbf{S}_{QRS}$, can be segmented by taking a 30 ms interval centered at $n_{R,p}^D$. That interval time was defined by their onset, $n_{R,o}^D$ and end $n_{R,e}^D$.

$$\mathbf{S}_{QRS} = [\mathbf{s}(n_{R,o}^D), \ldots, \mathbf{s}(n_{R,e}^D)] \tag{11}$$

The angle between repolarization and depolarization was estimated throughout the descriptor Total Cosine R-to-T (T_{CRT}) [23], which was calculated as

$$T_{CRT} = \frac{1}{n_{R,e}^D - n_{R,o}^D + 1} \sum_{n=n_{R,o}^D}^{n_{R,e}^D} \cos \angle(\mathbf{s}(n), \mathbf{s}(n_{T,p}^D)) \tag{12}$$

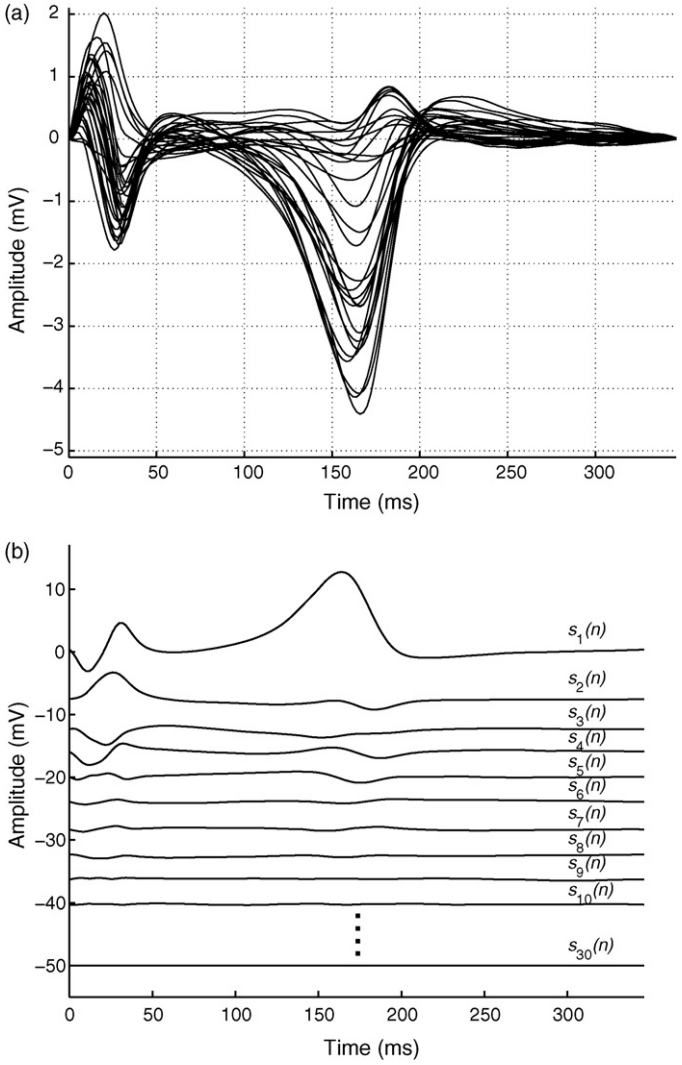

Fig. 4. 30 ECG recordings during control for DS protocol (top panel), and the first 10 and the 30th decomposed ECG signals (bottom panel). The signals were obtained by the projection of X onto $\mathbf{U}$.

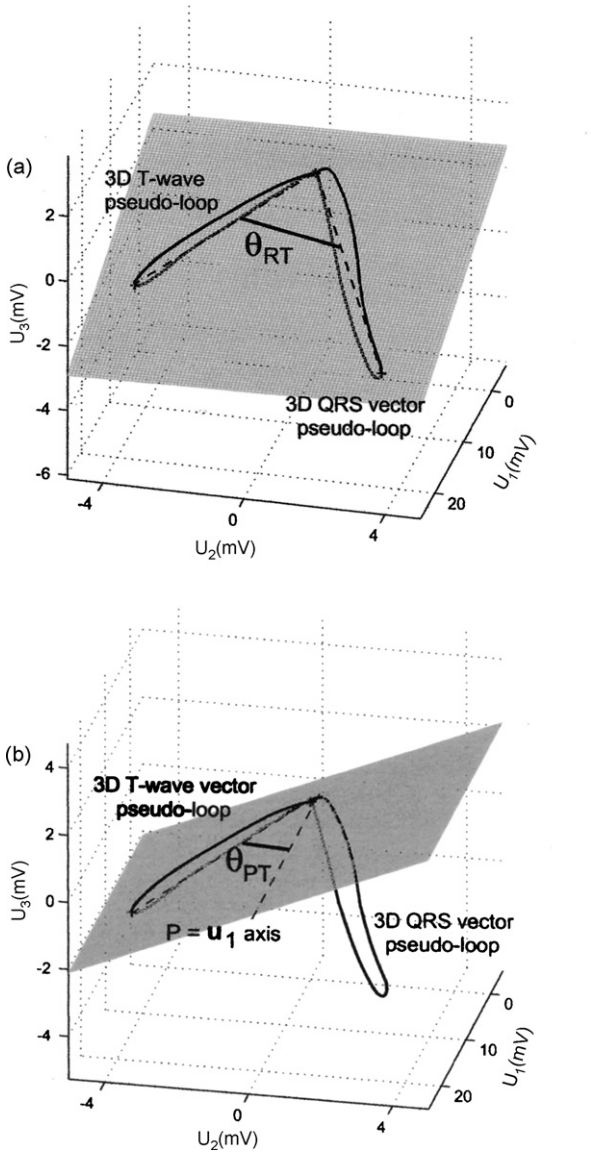

Fig. 5. QRS and T-wave vector pseudo-loops are shown for the angles (a) θ_{RT} and (b) θ_{PT}. θ_{RT} determines the angle between depolarization and repolarization phases, and θ_{PT} determines the angle between repolarization and a fix reference.

Previously, the $\mathbf{s}(n)$ vector have being normalized to have unity energy both at T-wave and QRS complexes. The depolarization and repolarization inscription vectors in the new 3D space obtained using ECG SVD were called pseudo-loops. Negative values indicate very large differences in the orientation of the QRS complex and T-wave pseudo-loops. We used as a performance index the angle $\theta_{RT} = \arccos(T_{CRT})$ (see Fig. 5a; however, if both vectors change in a similar way, this could not be reflected in the value of θ_{RT}. Given that the hypothesis predicts that only the T-wave vector varies with IVRD, we propose using an estimation of the angle between a fix reference and the T-wave as a VRD index, which avoids the uncertainties generated by a QRS pseudo-loop estimation [47]. The $\mathbf{u}_1$ in the three dipolar component subspace is denoted by $\mathbf{u}_1^D$ and has components $\mathbf{u}_1^D = [1, 0, 0]$. We propose the θ_{PT} angle as

$$\theta_{PT} = \angle(\mathbf{u}_1^D, \mathbf{s}(n_{T,p}^D)) = \text{arctg}\frac{\sqrt{s_2^2(n_{T,p}^D) + s_3^2(n_{T,p}^D)}}{s_1(n_{T,p}^D)} \quad (13)$$

obtained from the total cosine $\mathbf{u}_1^D$-axis to the T-wave vector angle. We take the principal component $\mathbf{u}_1^D$ from the control beat and use it as a reference axis in control and in IVRD conditions. θ_{PT} angle measures the mean difference of the repolarization axis with respect to the $\mathbf{u}_1^D$-reference in each beat experiment (see Fig. 5b).

(b) *T-wave residuum*, T_{WR}: We hypothesized that, if the IVRD is homogeneously generated across the myocardium, the dipolar model will remain valid and will not manifest differences at different levels of VRD [48], but T_W will. Therefore, we again calculated the SVD, but this time we used the $\mathbf{X}$ signal matrix restricted to the T-wave repolarization interval; thus, the signal array in Eq. (3) becomes

$$\mathbf{x}_{c,r} = [x_{c,r}(n_{T,o}^D), \ldots, x_{c,r}(n_{T,e}^D)]^T \quad (14)$$

The energy of the first three components of the SVD defined the dipolar components, c_d, and the non-dipolar components, c_{nd}, are thought to be due to regional heterogeneities and/or noise.

$$c_d = \sum_{i=1}^{3}\sigma_i^2 \quad \text{and} \quad c_{nd} = \sum_{i=4}^{M}\sigma_i^2 \quad (15)$$

To quantify the relative contribution of the c_{nd}, the the T-wave residuum index [25] is calculated as

$$T_{WR} = \frac{c_{nd}}{c_d + c_{nd}} \quad (16)$$

(c) *Measurement of the spatial T-wave morphology dispersion, T_{MD} and unnormalized T-wave morphology dispersion, UT_{MD}*: The ECGs matrix that corresponds to the repolarization was reconstructed from $\mathbf{S}_T$ as

$$\hat{\mathbf{X}}_T = \mathbf{U}_1\mathbf{S}_T \quad (17)$$

That is equivalent to a morphological filtering of the ECG signals, $\hat{\mathbf{X}}_T = \mathbf{U}_1\mathbf{S}_T = \mathbf{U}_1\mathbf{U}_1^T\mathbf{X}_T$. Then, we performed again the SVD decomposition of the $\hat{\mathbf{X}}_T$ expressed as

$$\hat{\mathbf{X}}_T = \mathbf{U}_T\Sigma_T\mathbf{V}_T^T = [\mathbf{U}_{T,1}\mathbf{U}_{T,2}]\begin{bmatrix}\Sigma_{T,1} & \mathbf{0}\\ \mathbf{0} & \Sigma_{T,2}\end{bmatrix}\begin{bmatrix}\mathbf{V}_{T,1}^T\\ \mathbf{V}_{T,2}^T\end{bmatrix}$$

where $\mathbf{U}_{T,1} \in \mathbb{R}^{M\times 2}$, $\Sigma_{T,1} \in \mathbb{R}^{2\times 2}$ and $\mathbf{V}_{T,1} \in \mathbb{R}^{2\times N}$. Thus, $\mathbf{U}_{T,1}$ is a matrix in which columns were the most significant left singular vector of $\hat{\mathbf{X}}_T$. $\mathbf{U}_{T,1} = [\mathbf{u}_{T,1}, \mathbf{u}_{T,2}]$, with $\mathbf{u}_{T,j} \in \mathbb{R}^{M\times 1}$. The third component of the SVD is neglected because it represents a small portion of the ECG energy [21]. Each row, $\mathbf{z}_{T,j}^T$, of $\mathbf{U}_{T,1} = [\mathbf{z}_{T,1}, \ldots, \mathbf{z}_{T,M}]^T$, $\mathbf{z}_{T,j} \in \mathbb{R}^{2\times 1}$, represents the reconstruction vector (Eq. (17)), which can be interpreted as the direction to which the SVD decomposed signal needs to be projected to recover an estimate of the original jth lead signal after the rank reduction performed by the SVD.

Table 1
Mean ± S.D. of the indexes obtained using temporal analyses

	C_{PVS}	D_{PVS}	$p <$	C_{DS}	D_{DS}	$p <$
T_o^A (ms)	123.8 ± 15.4	99.3 ± 18.8	0.005	137.0 ± 12.4	115.4 ± 34.6	0.022
T_p^A (ms)	162.1 ± 16.7	142.5 ± 13.7	0.005	169.4 ± 13.2	165.8 ± 27.1	NS
T_e^A (ms)	220.8 ± 14.8	217.8 ± 16.4	NS	215 ± 18.1	249.0 ± 25.4	0.005
T_W (ms)	95.2 ± 7.9	118.5 ± 15.7	0.007	78.0 ± 10.3	133.6 ± 29.6	0.005
T_M (mV)	1.7 ± 0.4	2.4 ± 0.8	0.028	2.2 ± 0.9	2.4 ± 0.9	NS
T_A (mV ms)	(3.8 ± 1.2) 10^4	(5.9 ± 2.3) 10^4	0.007	(5.7 ± 2.5) 10^4	(11.3 ± 6.0) 10^4	0.047

A $p < 0.05$ indicates a statistically significant difference.

We calculated the angle between each ($\mathbf{z}_{T,i}$ $\mathbf{z}_{T,j}$) pair of vectors, α_{ij} $(i, j = 1, \ldots, M; i \neq j)$ as

$$\alpha_{ij} = \angle(\mathbf{z}_{T,i}, \mathbf{z}_{T,j}) \in [0^\circ, 180^\circ] \quad (19)$$

which gives an indication of how the leads ith and jth differ in shape because a small angle means close reconstruction projection directions and then close shape and viceversa. We defined the UT_{MD} (unmormalized T-wave morphology dispersion) as the mean of all α_{ij}

$$UT_{MD} = \frac{1}{M(M-1)} \sum_{i,j=1;i\neq j}^{M} \angle(\mathbf{z}_{T,i}, \mathbf{z}_{T,j}) \quad (20)$$

The Eq. (20) differs from the definition of T_{MD} presented by Acar and Koymen [21]. In their work, the vectors from which the angles are estimated are the $\mathbf{z}_{T,i}$ after being rotated using weighting factors that are proportional to the eigenvalues $\Sigma_{T,1}$. In this work, we rather use the vector directions, that give the reconstruction projection direction according Eq. (17), are the $\mathbf{z}_{T,i}$, as in Eq. (20). UT_{MD} is a quantification of the variation in T-wave spatial morphology. We calculated UT_{MD1}, which is UT_{MD} restricted to the first half of the T-wave ($\mathbf{S}_T$ in Eq. (17) restricted between $n_{T,o}^D$ and $n_{T,p}^D$) and UT_{MD2}, which is the second half of the T-wave (between $n_{T,p}^D$ and $n_{T,e}^D$).

2.5.3. Analyses of ECG repolarization duration and dispersion variables

The standard ECG variables were analyzed semi-automatically by two experienced researches. The software allowed the ECG variables to be measured semi-automatically using a calibrated cursor with a time resolution of 1 ms. The variables are

- QT_p: Interval between the beginning of the QRS complex and the peak of the T-wave.
- QT_e: Interval between the beginning of the QRS complex and the end of the T-wave.
- Δ_{QT_p}: QT_p interval dispersion expressed as the difference between the maximum and minimum durations of the QT_p interval.
- Δ_{QT_e}: QT_e interval dispersion expressed as the difference between the maximum and minimum durations of the QT_e interval (which is known as QT_d).
- σ_{QT_p}: Standard Deviation of the QT_p interval.
- σ_{QT_e}: Standard Deviation of the QT_e interval.

2.6. Statistical analyses

Results are presented as mean ± standard deviation (S.D.). The non-parametric Wilcoxon test was used because the underlying distribution of the variables was unknown. When p was < 0.05, differences were considered statistically significant.

3. Results

The variables T_o^A, T_e^A, T_p^A, and T_W during the control condition and during the IVRD of 20 rabbit hearts are presented in Table 1. In addition, we compared the T_M and T_A of the control and IVRD conditions. The control and IVRD for indexes obtained from the SVD are presented in Table 2. In this table, we can see the dipolar and non-dipolar components and

Table 2
Mean ± S.D. of the indexes obtained using geometrical analyses

	C_{PVS}	D_{PVS}	$p <$	C_{DS}	D_{DS}	$p <$
c_d (mV^2)	(4.1 ± 2.1) 10^9	(8.1 ± 4.7) 10^9	0.009	(6.8 ± 5.3) 10^9	(16.2 ± 1.5) 10^9	NS
c_{nd} (mV^2)	(5.4 ± 3.6) 10^6	(18.8 ± 2.0) 10^6	0.005	(1.0 ± 1.4) 10^7	(2.7 ± 3.3) 10^7	NS
T_{WR} (%)	0.2 ± 0.1	0.3 ± 0.2	NS	0.1 ± 0.1	0.2 ± 0.2	NS
T_{MD} (°)	76 ± 14	76 ± 10	NS	49 ± 10	52 ± 27	NS
T_{MD1} (°)	75 ± 17	79 ± 12	NS	47 ± 10	49 ± 35	NS
T_{MD2} (°)	78 ± 15	78 ± 19	NS	50 ± 11	53 ± 26	NS
UT_{MD} (°)	77 ± 11	81 ± 6	NS	66 ± 8	63 ± 11	NS
UT_{MD1} (°)	35 ± 13	70 ± 15	0.005	66 ± 6	60 ± 8	NS
UT_{MD2} (°)	78 ± 12	81 ± 6	NS	51 ± 11	53 ± 27	NS
θ_{RT} (°)	149 ± 7	133 ± 22	NS	41 ± 17	73 ± 42	0.05
θ_{PT} (°)	137 ± 65	129 ± 61	NS	35 ± 51	117 ± 49	0.009

A $p < 0.05$ indicates a statistically significant difference.

Table 3
Mean ± S.D. of duration and dispersion variables obtained using classical analysis

	C_{PVS}	D_{PVS}	$p <$	C_{DS}	D_{DS}	$p <$
QT_p (ms)	201.6 ± 15.4	195.4 ± 24.9	NS	168.4 ± 10.9	180.7 ± 17.7	0.005
QT_e (ms)	256.1 ± 16.7	266.5 ± 26.9	0.037	209.8 ± 12.2	245.7 ± 20.7	0.005
Δ_{QT_p} (ms)	43.9 ± 13.9	58.6 ± 12.8	NS	30.1 ± 9.8	42.9 ± 8.1	0.005
Δ_{QT_e} (ms)	34.6 ± 11.8	59.9 ± 14.3	0.005	25.4 ± 5.4	48.10 ± 5.17	0.005
σ_{QT_p} (ms)	10.4 ± 3.6	14.7 ± 4.4	0.037	6.6 ± 2.2	11.9 ± 1.9	0.005
σ_{QT_e} (ms)	7.6 ± 2.2	13.0 ± 3.4	0.007	6.5 ± 1.4	11.6 ± 1.9	0.007

A $p < 0.05$ indicates a statistically significant difference.

their relationship, as well as the T-wave morphology dispersion and unnormalized T-wave morphology dispersion with the purpose of determining the similarity of the processes of repolarizacion of the *i*th and *j*th lead. Furthermore, the θ_{RT} and the new index proposed θ_{PT} were compared when IVRD condition. Table 3 shows the classical duration and dispersion variables of ventricular repolarization using the interlead differences of the QT interval duration [7].

4. Discussion

During cardiac depolarization and repolarization, local effects can occur that can not be well represented on the ECG using a dipolar model. That effect is more marked in regional pathological conditions. The T_{WR} is an index that aims to reflect the local heterogeneity of VRD through c_{nd}. In the experimental model used in our study, the T_{WR} index did not detect IVRD (see Table 2), probably because the premature beats and the d-Sotalol supply generated IVRD that was homogeneously distributed throughout the myocardium, and then well represented by the dipolar model. T_{WR} might be a good marker for IVRD, when the spatial heterogeneity of VRD is strictly localized in some myocardium areas.

Simultaneous increases in c_d and c_{nd} were observed in the PVS protocol. We hypothesized that, under abnormal repolarization, such as premature ventricular stimulation, an increase in the dipolar and non-dipolar components might be the expression of global IVRD contained within the T-wave. Hence, an increase, no change, or even a decrease in the relative T_{WR} could result depending on the magnitude of the changes associated with the two components. In the PVS experiment, the T_{WR} index did not change. On the other hand, in d-Sotalol experiment, even c_d and c_{nd} showed marked increases, but T_{WR} remained unchanged. It could be hypothesize that under heterogeneous anatomic damage to the heart (cardiomyopathies and myocardial infarction), an increase in the non-dipolar components and, consequently, an increase in the relative T_{WR} should be induced. In other pathologies, such as the proarrhythmic effects of class III antiarrhytmic agents, or during premature ventricular beats (which possibly generated homogeneous IVRD), an increase or no change in the dipolar and non-dipolar components could be manifested. In that case, the relative T_{WR} will not change.

In our study, the T-wave duration increased when the VRD was augmented (Table 1). The increase in T_W indicates a differential shortening or lengthening of the APD in some myocardium areas, reflecting the range of times at which action potentials are ending and, therefore, it could be considered an expression of the APD dispersion. In addition, other variables changed (Table 1). In PVS, T_o^A and T_p^A shortened to 25 and 20 ms, respectively, which indicates dispersion generated by early ending APD. T_e^A did not change significantly, nevertheless T_W duration increased significantly, which suggests different modifications of APD at different areas. T_o^A and T_e^A decreased 20 ms and increased 35 ms respectively, when DS was supplied, suggesting that DS generates both situations at different areas of the myocardium, ending APD early at some areas and delaying the ending at others.

Other authors [49] have shown, in isolated Langendorff-perfused rabbit heart, that QT interval of cardiac surface electrograms (interval from the initiation ventricular to the positive peak of the T-wave in the epicardial electrograms) was longer in the apical than the basal area. This specific measure reflected the APD in different places of the rabbit heart. They attributed this phenomena to the difference of density of I_K in the apical and basal myocytes of the rabbit left ventricle. Moreover, as well as in other species epicardial to endocardial differences in the repolarizating K^+ currents may also exist in rabbits ventricles [50].

In Fig. 1 we show the schematic picture representing the T-wave generation as a result of combined dispersion between apex to base and/or transmural APD. The IVRD due to any of these kinds could be result in T-wave widening. However, since no definitive evidences exist to what extend T-wave width in rabbits comes from transmural or apex to base dispersion, this picture should be seen just as a schematic to comprehend the hypothesis of the T-wave widening independently if it comes form one or other dispersion type.

Our results support the hypothesis that IVRD reflects a widening in the T-wave duration when IVRD is generated across the entire myocardium. In the PVS and DS protocols, T_W increased 23 ms and 55 ms, respectively. In our work, θ_{RT} and θ_{PT} did not appear as IVRD markers during PVS (Table 2), maybe because of the unstructured QRS complex at PVS, which reduces the significance of the dominant vector at depolarization and repolarization. However in the case of DS, θ_{RT} and θ_{PT} proved to be IRVD markers. The high statistical significance of θ_{PT} supports the hypothesis that the fixed reference to the experimental tank, better estimated the repolarization axis variation as VRD increased. That situation for θ_{PT} can be transfered easily to a human recording situation, just by using a fixed reference attached to the lead system, rather than to the R-wave.

During DS and PVS conditions, UT_{MD} did not differ significantly between control and IVRD, which suggests that this index is not affected by global IVRD. Only UT_{MD1}, which represented the ascending portion of the T-wave, differed significantly between the control and IVRD in PVS protocol. When the decomposition space was rescaled to equalize the energies in the two directions as $\mathbf{W}_{T,1} = [\mathbf{z}_{T,1}, \ldots, \mathbf{z}_{T,M}]^T$ $\Sigma_{T,1} = [\mathbf{w}_{T,1}, \ldots, \mathbf{w}_{T,M}]^T$, we recalculated the angle between each ($\mathbf{w}_{T,i}$ $\mathbf{w}_{T,j}$) pairs of vectors as was proposed in [23]. The indexes T_{MD}, T_{MD1} and T_{MD2} did not result in statistically significant changes in either of the two protocols.

Furthermore, assuming stable Q-wave onset across leads, QT_e and T_e^A, which represent total ventricular repolarization, have similar behavior when the VRD was increased artificially using DS, although QT_p and T_p^A did not developed similarly. Besides, when the VRD was increased using PVS, QT_e and T_e^A, and QT_p and T_p^A did not develop similarly. That might be because the QT was measured from the onset of the QRS complex, but the T_e^A is refered to the maximum upstroke of the QRS complex derivative. Maybe these two measures have different degrees of reliability, being the upstroke definition more stable, and the uncertainly in the QRS onset made the measures of QT_p and QT_e unreliable.

Results obtained when IVRD was calculated using classic variables ($\Delta_{QT_e}, \sigma_{QT_e}$, and σ_{QT_p}) showed significant statistically differences. The relevance of those variables has been questioned [22,25], which motivated us to introduce the T-wave width, which is, in our opinion, better than the QT_d from a physiological perspective. This behaviour, which identifies significant stratification, even if the physiological relationship between IVRD and QT_d is unclear, might occur because the IVRD produces a T-wave that has a greater width, but a similar amplitude, which makes the determination of the T end point less well defined (a more gradual T-wave transition to the baseline), resulting in greater variance from lead to lead, which is reflected in the QT_d parameters (Δ_{QT_e}, σ_{QT_e}). Note that the QT_d based on the QT peak did not cause significant differences or they were marginally significant (Δ_{QT_p}, σ_{QT_p}, see Table 3) during DS protocol. We emphasize that the C_V (see Section 2.3) showed very little variation over time for the variables that represent the durations of the depolarization and repolarization processes and T-wave morphology. For that reason, we conclude that such variations did not affect the global changes in repolarization.

5. Conclusions

The results of our study can be extrapolated to human ECG recordings based on the assumption that ECGs registered in the tank (volume conductor) behaved similarly to electrical activity recorded on the body surface. Even if there are differences to consider, overall behaviour and the hypothesis that the T-wave width is an indicator of VRD still holds, and our study demonstrated the convenience of evaluating this marker as indicator of IVRD in human ECG recordings. The simplicity of the calculation reinforces the virtue of this index. Finally, studies are needed to estimate the normal and pathological values of the new indexes, such as T_W and θ_{PT}. Besides, it could be important to find a gold standard of T_W and θ_{PT} to be independent of the control value of them in each case. In the present study the IVRD indexes are compared to its own control values, which will be difficult to determine in human subjects, unless an historical series of ECG recordings are present throughout the patients clinical history.

Acknowledgements

This work was partially supported by projects TEC2004-05263-c02-02 from MCyT and FEDER, Grupo Consolidado GTC from DGA (Spain), AECI ref: A/2232/04 (Spain) and PIP 5272 from IAM-CONICET (Argentina).

References

[1] C.S. Kuo, K. Munakata, P. Reddy, B. Surawicz, Characteristics and possible mechanism of ventricular arrhythmia dependent on the dispersion of action potential, Circulation (1983) 1356–1367.
[2] B. Surawicz, Ventricular fibrillation and dispersion of repolarization, J. Cardiovasc. Electrophysiol. 8 (1997) 1009–1012.
[3] J. Han, G.K. Moe, Nonuniform recovery of excitability in ventricular muscle, Circ. Res. 14 (1964) 44–54.
[4] J.A. Vassallo, D.M. Cassidy, K.E. Kindwall, F.E. Marchlinski, M.E. Josephon, Nonuniform recovery of excitability in the left ventricle, Circulation 78 (1988) 1365–1372.
[5] W. Shimizu, C. Antzelevitch, Sodium channel block with mexiletine is effective in reducing dispersion of repolarization and preventing torsades de pointes in *LQT*2 and *LQT*3 models of the long-*QT* syndrome, Circulation 96 (1997) 2038–2047.
[6] W. Shimizu, C. Antzelevitch, Cellular basis for the *ECG* features of the *LQT*1 form of the long *QT* syndrome. Efects of β adrenergic agonist and antagonist and sodium channel blockers on transmural dispersion of repolarization and torsades de pointes, Circulation 98 (1998) 2314–2322.
[7] C.P. Day, J.M. McComb, R.W.F. Campbell, *QT* dispersion: an indication of arrhythmia risk in patients with long *QT* intervals, Br. Hearts J. 1 (1990) 335–343.
[8] K. Hnatkova, M. Malik, J. Kautzner, Y. Guang, A.J. Camm, Adjustment of *QT* dispersion assessed from 12 lead electrocardiograms for different number of analysed electrocardiographic leads: Comparison of stability of different methods, Br. Heart J. 72 (1994) 390–396.
[9] G. Yi, X.H. Guo, R. Crook, K. Hnatkova, A.J. Camm, M. Malik, Computerised measurements of *QT* dispersion in healthy subjects, Heart 80 (1998) 459–466.
[10] J.C. Cowan, K. Yusoff, M. Moore, P.A. Amos, J.P. Bourke, S. Tansuphaswadikul, R.W. Campbell, Importance of lead selection in *QT* interval measurement, Am. J. Cardiol. 61 (1988) 83–87.
[11] M. Zabel, S. Portnoy, M.R. Franz, Electrocardiographic indexes of dispersion of ventricular repolarization: An isolated heart validation study, J. Am. Coll. Cardiol. 25 (1995) 746–752.
[12] M. Zabel, P.R. Lichtlen, A. Haverichl, M.R. Franz, Comparison of *ECG* variables of dispersion of ventricular repolarization with direct myocardial repolarization measurements in the human heart, J. Cardiovasc. Electrophysiol. 9 (1998) 1279–1284.
[13] S.G. Priori, C. Napolitano, L. Diehl, P.J. Schwartz, Dispersion of the *QT* interval. a marker of therapeutic efficacy in the idiopathic long-*QT* syndrome, Circulation 89 (1994) 1681–1689.
[14] S.H. Hohnloser, A. van de Loo, D. Kalusche, W. Arents, B. Quart, Does sotalol-induced alteration of *QT* dispersion predict effectiveness or proarrhythmic hazards? Circulation 88 (Suppl. I:1) (1993) 392.
[15] J. Kautzner, Y. Gang, A.J. Camm, M. Malik, Short and long-term reproducibility of *QT*, *QT*c and *QT* dispersion measurement in healthy subjects, PACE Pacing Clin. Electrophysiol. 17 (1994) 928–937.

[16] P.W. Macfarlane, S.C. McLaughin, J.C. Rodger, *QT* dispersion: evidence to favor a vectorial component, J. Am. Coll. Cardiol. 29 (suppl.) (1997) 148A.
[17] J.A. Kors, G. van Herpen, J.H. van Bemmel, *QT* dispersion as an attribute of *T*-loop morphology, Circulation 99 (1999) 1458–1463.
[18] P. Langley, D. Di Bernardo, A. Murray, Comparison of three measures of *QT* dispersion, Comput. in Cardiol., IEEE Comput. Soc. 29 (1999) 69–72.
[19] P.W. Macfarlane, S.C. McLaughlin, C. Rodger, Influence of lead selection and population on automated measurement of *QT* dispersion, Circulation 98 (1998) 2160–2167.
[20] K.W. Lee, P. Kligfield, P.M. Okin, G.E. Dower, Determinants of precordial *QT* dispersion in normal subjects, J. Electrocardiol. 31 (Suppl.) (1998) 128–133.
[21] B. Acar, H. Koymen, *SVD* based on line exercise *ECG* signal orthogonalization, IEEE, Trans. Biomed. Eng. 46 (3) (1999) 311–321.
[22] M. Zabel, M. Malik, K. Hnatkova, M.D. Papademetriou, A. Pittaras, R.D. Fletcher, M.R. Franz, Analysis of *T*-wave morphology from the 12-lead electrocardiogram for prediction of Long-Term prognosis in male *US* veterans, Circulation 105 (2002) 1066–1070.
[23] B. Acar, G. Yi, K. Hnatkova, M. Malik, Spatial, temporal and wavefront direction characteristics of 12-lead *T*-wave morphology, Med. Biol. Eng. Comput. 37 (1999) 574–584.
[24] S. Priori, D. Mortara, C. Napolitano, L. Diehl, V. Paganini, F. Cant, G. Cant, P. Schwartz, Evaluation of the spatial aspects of *T* wave complexity in the long-*QT* syndrome, Circulation 96 (1997) 3006–3012.
[25] M. Malik, B. Acar, Y. Gang, Y.G. Yap, K. Hnatkova, A.J. Camm, *QT* dispersion does not represent electrocardiographic interlead heterogeneity of ventricular repolarization, J. Cardiovasc. Electrophysiol. 11 (2000) 835–843.
[26] P. Smetana, V. Batchvarov, K. Hnatkova, A.J. Camm, M. Malik, Ventricular gradient and nondipolar repolarization components increase at higher heart rate, Am. J Physiol. Heart Circ. Physiol. 286 (2004) H136.
[27] M.S. Fuller, G. Sándor, B. Punske, B. Taccardi, R. MacLeod, P.R. Ershler, L.S. Green, R.L. Lux, Estimation of repolarization dispersion from electrocardiographic measurements, Circulation 102 (2000) 685–691.
[28] D. Noble, I. Cohen, The interpretation of the *T* wave of the electrocardiogram, Cardiovasc. Res. 12 (1978) 13–27.
[29] G. Yan, M. Jack, Electrocardiographic *T* wave: A symbol of transmural dispersion of repolarization in the ventricles, J. Cardiovasc. Electrophysiol. 14 (2003) 639–640.
[30] G. Yan, C. Antzelevitch, Cellular basis for the normal *T* wave and the electrocardiographic manifestation of the long-*QT* syndrome, Circulation 98 (1998) 1928–1936.
[31] M. Zabel, S.H. Hohonloser, S. Beherens, R.L. Woosley, M.R. Franz, Differential effects of d-Sotalol, quinidine and amiodarone on dispersion of ventricular repolarization in the isolated rabbit heart, J. Cardiovasc. Electrophysiol. 8 (1997) 1239–1245.
[32] P.D. Arini, R.A. Quinteiro, E.R. Valverde, G.C. Bertrán, M.O. Biagetti, Evaluation of *QT* interval dispersion in a multiple electrodes recording system versus 12-lead standard *ECG* in an in vitro model, A. Noninv. Electrocardiol. 5 (2) (2000) 125–132.
[33] C.S. Kuo, J.P. Amlie, K. Munakata, C.P. Reddy, B. Surawicz, Dispersion of monophasic action potential durations and activation times during atrial pacing, ventricular pacing, and ventricular premature stimulation in canine ventricles, Cardiovasc. Res. 17 (1983) 152–161.
[34] D.S. Rosenbaumm, D.T. Kaplan, A. Kanai, L. Jackson, H. Garan, R.J. Cohen, G. Salama, Repolarization inhomogeneities in ventricular myocardium change dynamically with abrupt cycle length shortening, Circulation 84 (1991) 1333–1345.
[35] S. Yuan, C. Blomström-Lundqvist, C. Pherson, B. Wohlfart, S.B. Olsson, Dispersion of ventricular repolarization following double and triple programmed stimulation: A clinical study using the monophasic action potential recording technique, Eur. Heart J. 17 (1996) 1080–1091.
[36] A. Dabrowski, E. Kramarz, R. Piotrowicz, Dispersion of *QT* interval in premature ventricular beats as a marker of susceptibility arrhythmic events, J. Cardiovasc. Risk 25 (1998) 746–752.
[37] P.D. Arini, R.A. Quinteiro, E.R. Valverde, G.C. Bertrán, M.O. Biagetti, Differential modulation of electrocardiographic indices of ventricular repolarization dispersion depending on the site of pacing during premature stimulation, J. Cardiovasc. Electrophysiol. 12 (2001) 36–42.
[38] K.R. Laurita, S.D. Girouard, G.A. Fadi, D.S. Rosenbaum, Modulated dispersion explains changes in arrhythmia vulnerability during premature stimulation of the heart, Circulation 98 (1998) 2774–2780.
[39] C. Antzelevitch, W. Shimizu, G.X. Yan, S. Sicouri, W.J.V. Nesterenko, A. Burashnikov, J. Di Diego, J. Saffitz, G.P. Thomas, The *M* cell: Its contribution to *ECG* and to normal and abnormal electrical function of the heart, J. Cardiovasc. Electrophysiol. 10 (1999) 1124–1152.
[40] K.R. Laurita, S.D. Girouard, D.S. Rosenbaum, G.A. Fadi, Modulation of ventricular repolarization by a premature stimulus: Role of epicardial dispersion of repolarization kinetics demonstrated by optical mapping of the intact guinea pig heart, Circ. Res. 79 (1996) 493–503.
[41] J. Spear, E. Moore, Modulation of arrhytmias by isoproterenol in a rabbit heart model of d-Sotalol induced long *QT* intervals, Am. J. Physiol 279 (2000) H15–H25.
[42] B. Rosner, Fundamentals of Biostatistics, fourth ed., Duxbury Press, 1994 .
[43] P. Laguna, N.V. Thakor, P. Caminal, R. Jané, H.R. Yoon, A new algorithm for *QT* interval analysis in 24-h holter *ECG*: perfomance and applications, Med. Biol. Comput. 28 (3) (1990) 67–73.
[44] C.R. Meyer, H.N. Keiser, Electrocardiogram baseline noise estimation and removal using cubic spline and state-space computation techniques, Comput. Biomed. Res. 10 (1977) 459–470.
[45] D.B. Geselowitz, Dipole theory in electrocardiography, Am. J. Cardiol. 14 (1964) 301–306.
[46] A.M. Scher, A.C. Young, W.M. Meredith, Factor analysis of the electrocardiogram. Test of electrocardiographic theory: normal hearts, Circ. Res. VIII (1959) 519–526.
[47] P.D. Arini, E.R. Valverde, G.C. Bertrán, P. Laguna, Geometrical and temporal *ECG* features for quantification of increased ventricular repolarization dispersion in an experimental heart rabbit model, in: XXXII International Conference on Comp. in Cardiol., IEEE Computer Society 32, 2005, 89–92.
[48] P.D. Arini, E.R. Valverde, G.C. Bertrán, P. Laguna, Quantification of ventricular repolarization dispersion on the electrocardiogram by means of *T* wave duration, XXXI International Conference in Comp. in Cardiol., IEEE Comput. Soc. 31 (2004) 757–760.
[49] H. Iwata, I. Kodama, R. Suzuki, K. Kamiya, J. Toyama, Effects of Long-term oral administration of amiodarone on the ventricular repolarization of rabbits hearts, Jpn. Circ. J. 60 (1996) 662–672.
[50] J. Cheng, K. Kamiya, W. Liu, Y. Tsuji, J. Toyama, I. Kodama, Heterogeneous distribution of the two components of delayed rectifier K^+: a potential mechanism of the proarrhytmic effects of methanesulfonanilide class *III*, Cardiovasc. Res. 43 (1999) 135–147.